Lab on a Chip

PAPER

View Article Online
View Journal | View Issue

Cite this: *Lab Chip*, 2024, **24**, 4344

Controlling bacterial growth and inactivation using thin film-based surface acoustic waves†

Hui Ling Ong, [a] Bruna Martins Dell' Agnese,[b] Yunhong Jiang,[b] Yihao Guo,[c] Jian Zhou, [c] Jikai Zhang,[a] Jingting Luo,*[ad] Ran Tao, [ad] Meng Zhang,[b] Lynn G. Dover,[b] Darren Smith, [b] Kunyapat Thummavichai, [a] Yogendra Kumar Mishra, [e] Qiang Wu [a] and Yong-Qing Fu *[a]

Formation of bacterial films on structural surfaces often leads to severe contamination of medical devices, hospital equipment, implant materials, *etc.*, and antimicrobial resistance of microorganisms has indeed become a global health issue. Therefore, effective therapies for controlling infectious and pathogenic bacteria are urgently needed. Being a promising active method for this purpose, surface acoustic waves (SAWs) have merits such as nanoscale earthquake-like vibration/agitation/radiation, acoustic streaming induced circulations, and localised acoustic heating effect in liquids. However, only a few studies have explored controlling bacterial growth and inactivation behaviour using SAWs. In this study, we proposed utilising piezoelectric thin film-based SAW devices on a silicon substrate for controlling bacterial growth and inactivation with and without using ZnO micro/nanostructures. Effects of SAW powers on bacterial growth for two types of bacteria, *i.e.*, *E. coli* and *S. aureus*, were evaluated. Varied concentrations of ZnO tetrapods were also added into the bacterial culture to study their effects and the combined antimicrobial effects along with SAW agitation. Our results showed that when the SAW power was below a threshold (*e.g.*, about 2.55 W in this study), the bacterial growth was apparently enhanced, whereas the further increase of SAW power to a high power caused inactivation of bacteria. Combination of thin film SAWs with ZnO tetrapods led to significantly decreased growth or inactivation for both *E. coli* and *S. aureus*, revealing their effectiveness for antimicrobial treatment. Mechanisms and effects of SAW interactions with bacterial solutions and ZnO tetrapods have been systematically discussed.

Received 1st April 2024,
Accepted 18th July 2024

DOI: 10.1039/d4lc00285g

rsc.li/loc

1. Introduction

Biofilms or bacterial films formed on structural surfaces become critical issues in hospital environments, especially for biomedical devices such as valves, catheters, and implants, and *E. coli* and *S. aureus* are two well-known bacteria associated with infectious diseases.[1–4] The survival rate of these bacteria species is influenced by intrinsic factors such as genetic mechanisms and metabolism, or external factors such as environmental conditions including the pH value, temperature and humidity.[5–8] For preventing bacterial film growth, various passive and active methods have been implemented. The common passive methods include prevention and/or inhibition of bacteria adhesion/biofilm formation on surfaces by using antibacterial/antifouling surfaces or multifunctional coatings.[9–12] However, the passive surfaces or coatings would not easily cause effective bacterial resistance, and often be easily damaged *in vivo* because the plasma proteins from biological fluids are easily transported back onto the surfaces, thereby inducing bacteria colonization and reducing their antibacterial effects.[9,13,14]

Active methods include those using ultraviolet (UV) light, laser irradiation, ultrasound, and addition of antibacterial agents such as antibiotics, antimicrobial peptides (AMPs), and silver ions (Ag^+), or zinc oxide (ZnO) micro- or nanostructures, and they have also been commonly used to eliminate the adhered bacteria on different surfaces.[9,15–18] However, there have been various issues such as effectiveness and efficiency of these methods, instability and toxicity aspects with AMPs, or increased concerns with safety and

[a] *Faculty of Engineering and Environment, Northumbria University, Newcastle upon Tyne, NE1 8ST, UK. E-mail: luojt@szu.edu.cn, Richard.fu@northumbria.ac.uk*
[b] *Hub of Biotechnology in the Building Environment, Department of Applied Science, Northumbria University, Newcastle upon Tyne, NE1 8ST, UK*
[c] *College of Mechanical and Vehicle Engineering, Hunan University, Changsha 410082, China*
[d] *Key Laboratory of Optoelectronic Devices and Systems of Ministry of Education and Guangdong Province, College of Physics and Optoelectronic Engineering, Shenzhen University, Shenzhen, 518060, China*
[e] *Smart Materials, NanoSYD, Mads Clausen Institute, University of Southern Denmark Alison 2, DK-6400, Sønderborg, Denmark*

† Electronic supplementary information (ESI) available. See DOI: https://doi.org/10.1039/d4lc00285g

toxicity when utilising nanoparticles.[19–21] Ultrasound has been studied as a method to stimulate and enhance the growth of biological substances and microbial cells.[22–26] Strong shear and mechanical stresses are generated by low frequency (in the kHz range) and high energy powered ultrasound for cleaning or mixing processes.[22,27,28] Meanwhile, high frequency (at sub-MHz and MHz levels) and low power density ultrasound is extensively employed in applications such as in diagnosis and imaging. The latter one has also been used for applications which require a huge quantity of redox radicals, such as the oxidation of organic contaminants in aqueous environments that involve large amounts of oxidising radicals.[22,27,28]

More recently, surface acoustic waves (SAWs) have been developed to realise biosensing and actuation functions which are based on acoustic wave propagation and vibrations on structural surfaces such as $LiNbO_3$, silicon, polymers, metal or glass.[29–32] SAWs have been widely utilised in various applications such as wireless communications, acoustofluidics, sensing, and particle/biological manipulations.[31,33–35] When compared to conventional ultrasound transducers, SAW devices exhibit various unique advantages which include minimised cell destructive, localised heating effect, miniaturized dimensions, low effect of cavitation, *etc.*[36] In fact, the less destructive and localised self-heating effects from SAWs are exceptionally critical for bacterial studies. As compared to conventional ultrasound transducers, SAW energy is mainly confined within the surface or sub-surface of the material where heat dissipation mainly occurs at one or a few wavelength depth from the surface.[36–38] Moreover, since conventional ultrasound transducers tend to be operated at lower frequencies than SAW devices, it was reported that higher frequencies are unlikely to generate significant cavitation effects on cell membranes thus not triggering cell death disrupting cell membranes.[36,39–42] Thin film-based SAWs have recently been widely investigated, with their advantages for realising bendable/flexible lab-on-a-chip (LOC) platforms and implementing highly integrated functions with microelectronics or other microfluidic/sensing approaches.[32,43] In addition to this, thin film-based SAW devices can be used directly onto structural surfaces such as glass, polymers, silicon, or metal to produce acoustic wave propagation and surface vibrations.[35,44] With all these excellent attributes, thin film-based SAWs should be suitably integrated for bacterial studies, in terms of bacterial growth and bacterial inactivation.

There are just a few previous studies using SAWs for bacteria inactivation. For example, Kopel *et al.* (2011) reported that low-energy SAWs create an elliptical movement and microstreaming in the medium, thus eradicating biofilm-residing bacteria when applied with an antibiotic simultaneously.[3] Loike *et al.* (2013) reported that SAWs can eradicate bacteria in a planktonic state and within biofilms.[1] Kazan *et al.* (2006) reported that low energy SAWs are effective towards the prevention of microbial biofilm formation.[45] It was also mentioned that the SAWs were repulsive to bacteria and interfered with/prevented the docking and adhesion of bacteria to solid surfaces, which were in the early stages of microbial biofilm growth.[45] Chew *et al.* reported that the acoustic radiation force induced on bacteria was the dominant mechanism for bacterial inactivation and they observed a 75% reduction in bacterial load in 10 min treatment with the highest SAW excitation power of 348 mW.[46] Hong *et al.* reported that biofilm formation was strongly affected by the flows in the thin layers of bacterial suspensions which were facilitated by surface waves.[47] Moreover, they discussed the various wave patterns which can either promote biofilm formation or prevent attachment of bacteria or biofilm formation.[47]

Although there are a lot of studies using SAWs for combating and eliminating bacteria biofilm formation in the literature, there have been few studies for the key mechanisms behind the interactions of SAWs and bacteria, with or without semiconducting material microparticles such as ZnO. It is unclear how SAWs affect the bacteria life cycle under these conditions, *i.e.*, conditions under which bacteria growth and control are enhanced or eliminated with SAW agitation. In this paper, the bacterial growth (using *E. coli* and *S. aureus* as two examples) and antibacterial performance using thin film SAW ZnO/Si devices were studied with and without using ZnO tetrapods. First, we investigated the effects of various applied SAW powers (ranging from 0.36 to 14.0 W) on bacteria growth and evaluated the rate of growth or inactivation in a polydimethylsiloxane (PDMS) chamber. Subsequently, we applied varied concentrations of ZnO tetrapods (2 to 4 mg mL^{-1}) in the bacteria solution within the chamber as presented in Fig. 1. The mechanisms of bacteria growth/inhibition and antibacterial performance using SAWs with ZnO tetrapod structures have been systematically studied.

2. Experimental details

2.1 Preparation and characterisation of SAW devices

ZnO films with ~4.5 μm thickness were deposited onto 4-inch (100)-orientated silicon substrates using a direct current (DC) reactive magnetron sputtering (NS3750, Nordiko) process in an ultra-high vacuum system. The base pressure of the chamber was 1×10^{-4} Pa before deposition. A zinc target with a purity of 99.999% was used for deposition of the ZnO films with a 20 cm distance from the substrate. During the deposition process, the surface of the substrate was pre-cleaned by means of short bombardment (5 min) with Ar ions using a DC power of 300 W. The deposition conditions were as follows: DC sputtering power of 400 W; Ar/O_2 mixing flow ratio of 10/15 SCCM (standard cubic centimetre per minute); deposition rate of ~750 nm h^{-1} with a deposition pressure of 1 Pa.

Interdigital transducers (IDTs) were patterned and fabricated on the ZnO thin films using a conventional photolithography and lift-off process. A bilayer of Cr/Au with

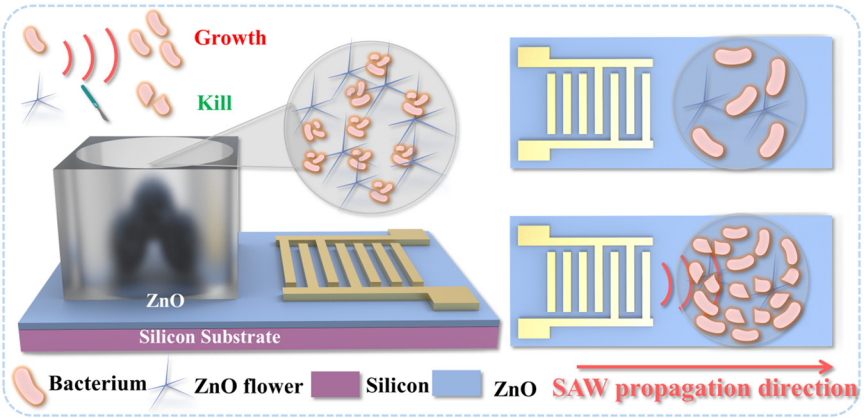

Fig. 1 An illustration of a PDMS chamber on a ZnO/Si SAW device for bacterial studies with thin film SAWs.

thicknesses of 20 nm/100 nm was prepared as the electrode in this study. Each IDT has 50 pairs of fingers, with a wavelength of 300 μm. The resonant characteristics (frequency and *S*-parameters) of the ZnO/Si SAW devices were measured using an RF vector network analyser (Keysight, FieldFox N9913A). An RF signal at the resonant frequency of the ZnO/Si SAW device was generated using a signal generator (Aim TTi, TG5011A) and then amplified using a power amplifier (Amplifier Research, Model 75A250). The RF power applied to the IDTs of the SAW devices was measured using an RF power meter (Racal Instruments 9104).

For evaluation of the induced surface heating effects upon SAW agitation, an infrared (IR) camera (FLIR, T620bx) was used to monitor the temperature changes on the SAW device at different RF powers. A K-type thermocouple was also used on the SAW device's surface to compare with and verify the results obtained from the IR camera. The temperature measurement was taken in front of the IDT area, where the bacteria solution was located during the testing. In addition, the temperature measurements at each of the RF powers were taken in triplicate during the SAW agitation, and it is worth noting that both the IR camera and the thermocouple showed nearly identical temperature readings during SAW agitation.

2.2 Processing and characterisation of ZnO tetrapods

Preparation methods of the ZnO tetrapods were reported previously in the literature.[48–50] Briefly, they were fabricated *via* the flame transport synthesis (FTS) technique which was a single-step process to convert Zn metallic particles directly into ZnO tetrapods. In a conventional FTS process, a mixture of Zn tetrapods (from Goodfellow, Huntington, UK) with an average diameter of 5 mm and poly(vinyl butyral) (PVB) powder (Mowital B 60H from Kuraray Europe GmbH, Hattersheim, Germany) at a weight ratio of 1 : 2 was first placed into a ceramic crucible and then heated to 900 °C in a furnace.[48,50] The PVB polymer in this instance acted as a sacrificial layer that was decomposed at a high temperature during the heating process in the furnace. During the heating process, the Zn microparticles were converted into Zn atomic vapour, which participated in the nucleation and growth processes of tetra-ZnO micro- and nanostructures *via* a solid–vapour–solid growth mechanism with the presence of native oxygen molecules.[48,49] The growth of fluffy tetra-ZnO micro- and nanostructure networks with higher aspect ratios was achieved when the sacrificial polymer was replaced with a process that involved heating Zn powder under a nitrogen atmosphere.[48–50]

The ZnO tetrapods were analysed based on their crystal structures using X-ray diffraction (XRD, D5000, Siemens, Cu-Kα radiation, 40 kV, 30 mA), utilising a Cu-Kα radiation source (λ = 0.15406 nm) operated at 2 kW. The ZnO microstructure solution was then prepared *via* dissolving the tetra-ZnO structures in deionised (DI) water with a concentration ranging from 2 to 4 mg mL^{-1}. The ZnO solution was ultrasonically mixed for 1 hour to achieve a homogeneous mixture. The morphology of these ZnO tetrapods was observed using a scanning electron microscope (SEM, Tescan Mira 3).

2.3 Bacterial culture of *E. coli* and *S. aureus*

Escherichia coli K12 (*E. coli*, DSMZ 3925) and *Staphylococcus aureus* (*S. aureus*, DSM 2569) were grown in a Luria Bertani (LB) broth overnight in a static incubator (37 °C) for 16 hours. From the culture, 1 mL of the bacteria solution was placed into a fresh 50 mL LB broth in an orbital shaking incubator at 37 °C for about 3 hours. Once this was done, the optical density (OD_{600}) value of the bacteria solution was measured. To obtain the standard growth curves for both bacteria cultures, the inocula for both cultures were standardised to an OD_{600} value of 0.01 and were placed in a Tecan plate reader. In addition, the LB broth was used as the control group. The OD_{600} measurements were taken hourly over a period of 24 hours.

2.4 SAW agitation and bacterial growth tests

The PDMS chamber was fabricated by using PDMS elastomers, Sylgard® 184 from Dow Corning®, with vinyl groups (part A) and hydrosilane groups (part B) in a ratio of

10 : 1. Once the mixture was completed, it was placed in a Petri dish where de-gassing was conducted inside a gas chamber. After the degassing process, the PDMS mixture was placed in an oven at 60 °C for 4 hours before it was cut into multiple 3 × 3 × 3 cm^3 cubes.

To evaluate the microbial growth under SAW agitation, OD measurements and cultivation in LB agar plates were performed for bacteria quantification. For the OD_{600} measurements, a bench-top spectrophotometer (WPA Biowave, CO8000 Cell Density Meter) was used. An aliquot of 3 mL of fresh *E. coli*/*S. aureus* inocula (OD_{600} 0.5, 10^7/10^8 CFU mL^{-1}) was placed inside the PDMS chamber, and they were divided into two groups: the SAW test group which was exposed to nine RF powers (0.36, 0.95, 1.4, 1.9, 2.55, 3.21, 4.01, 6.64, and 7.8 W) and the control, which was not exposed to any SAW agitation. Both the PDMS chambers for the control and test groups were used at room temperature. Different powers were evaluated individually for 30 minutes, and the inocula in the PDMS chamber were replaced in each subsequent test to maintain the initial OD_{600} at 0.5. At the end of 30 minutes, an aliquot (10 μL) of the bacteria solution was taken from the PDMS chamber for serial dilution in a 96 well plate, and 5 μL solution were drop cast onto LB agar plates from both the test and control groups to carry out bacterial quantification. After this process, the LB agar plates were incubated at 37 °C for overnight. To obtain the CFU mL^{-1} (colony forming unit per mL) value, the following equation was utilised:

$$\text{CFU mL}^{-1} = \frac{\text{Number of colonies} \times \text{dilution factor}}{\text{volume of culture plated in mL}} \quad (1)$$

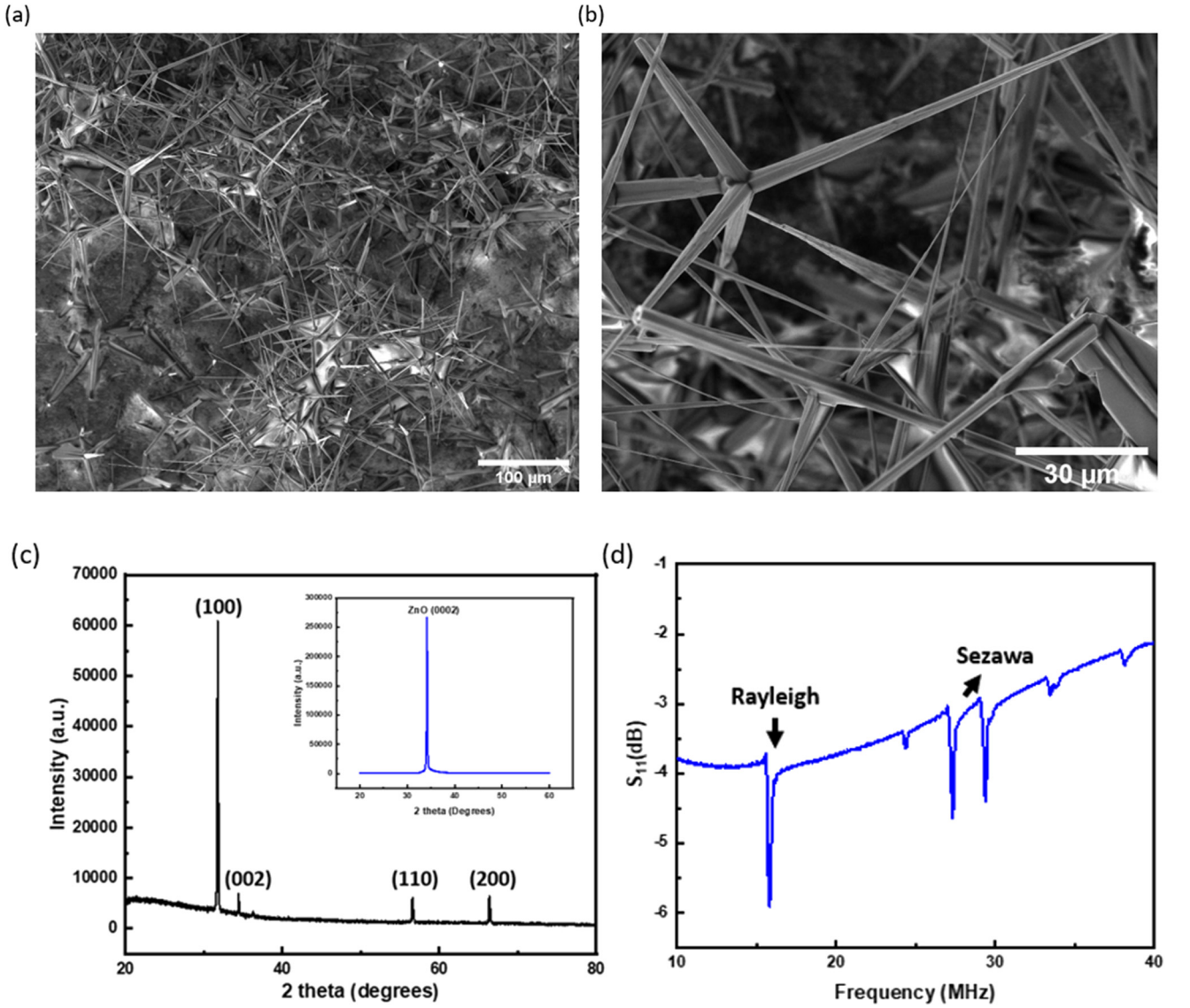

Fig. 2 (a) and (b) SEM images of ZnO tetrapods used; (c) XRD diffractogram of ZnO tetrapods, with an inset of the XRD diffractogram for the ZnO thin film; (d) frequency response (S_{11}) of the ZnO/Si SAW device with a wavelength of 300 μm.

2.5 ZnO tetrapods combined with SAWs

After SAW tests, *E. coli* and *S. aureus* cells were evaluated for antibacterial assays using ZnO tetrapods combined with SAWs. Following the similar conditions set for SAW tests previously mentioned, microbial inocula at OD_{600} 0.5 (control and test groups) were placed inside the PDMS chamber, in which three concentrations of ZnO tetrapods (2, 3, and 4 mg mL^{-1}) were added to the culture, with five RF powers applied for the SAW testing groups. After 30 minutes for each RF power tested, OD measurements and microbial quantification through serial dilutions and cultivation in LB agar plates were carried out. The plates were incubated at 37 °C, for 16 hours and quantified in CFU mL^{-1}.

3. Results and discussion

3.1 Characterisation of ZnO tetrapods and SAW devices

The SEM images of the ZnO tetrapod structures are shown in Fig. 2(a) and (b) at low and corresponding high magnifications, respectively. The average diameter of the ZnO arms is in the range of a few 100 nm to a few micrometres. Each tetrapod consists of four arms converging from the centre with angles of ~105° to 110°. This structure combines the features of one-dimensional ZnO micro and nanorods, which results in a highly porous linked network with numerous interconnecting (bridging) junctions.[48] The tetrapodal shape of these nanostructures is very effective in the construction of flexible, structurally intact, and mechanically stable 3D networks with very high porosities (up to 98%) and large surface-to-volume ratios, hence prompting the interaction between ZnO tetrapods and bacteria, along with SAWs.

The obtained XRD diffractograms of the ZnO tetrapods and ZnO thin film are shown in Fig. 2(c), and all the observed peaks are in accordance with those of wurtzite-type ZnO (JCPDS 36-1451). The sputtered ZnO film has a strong texture along the (0002) orientation, which is good for Rayleigh acoustic wave generation and propagation. The obtained dominant reflections of ZnO tetrapods, *e.g.*, the three theta peaks at 31.9°, 33.9° and 57.9°, are attributed to the (10–10), (0002) and (10–11) planes of the wurtzite ZnO.[48]

Fig. 2(d) shows the obtained reflection spectra (S_{11}) of the ZnO/Si SAW device with a wavelength of 300 μm. The

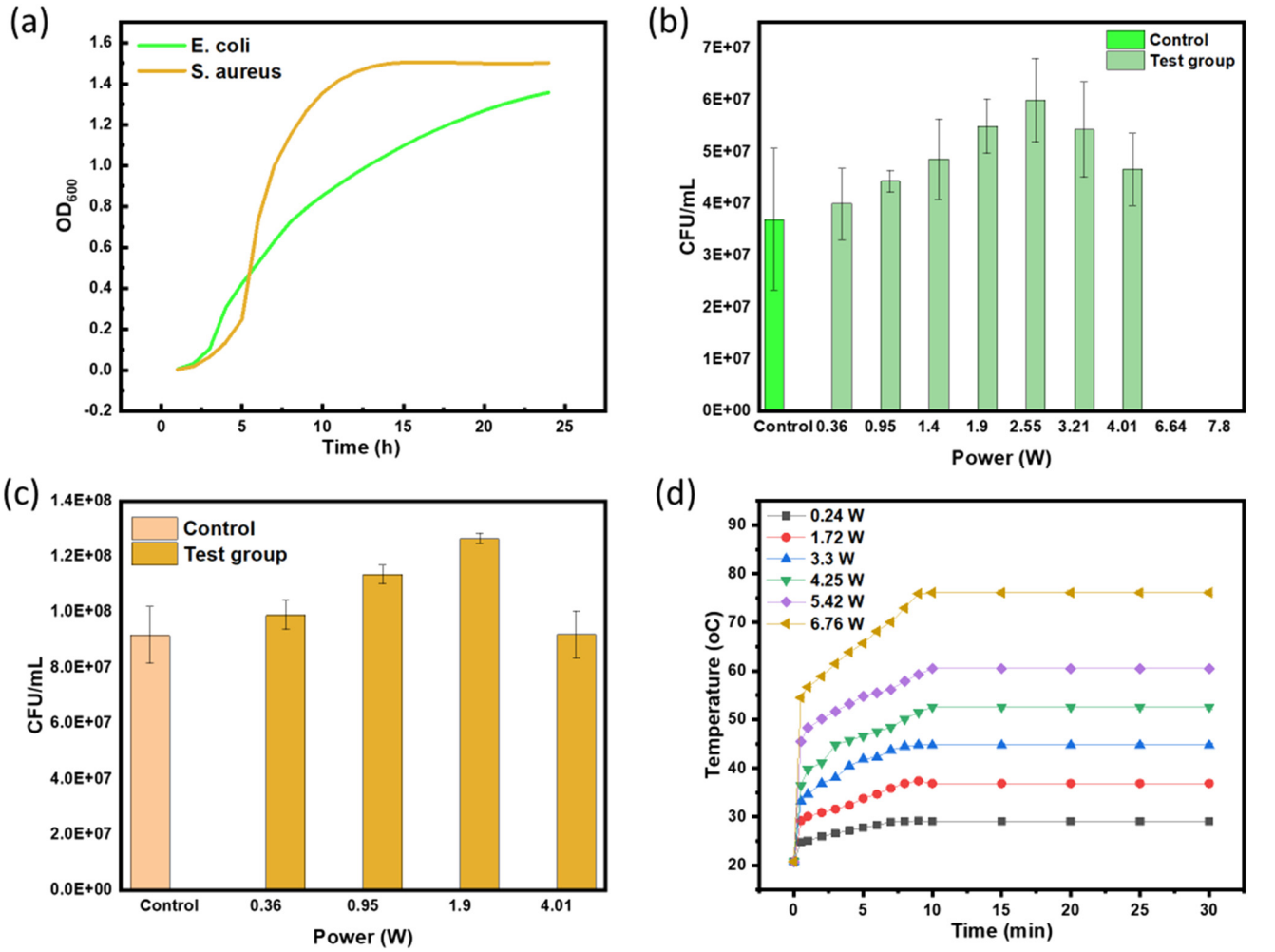

Fig. 3 OD measurements of (a) the standard curves of *E. coli* with and without SAWs; CFU mL^{-1} readings for (b) *E. coli* and (c) *S. aureus*; (d) temperature readings at different RF powers.

resonant frequency of the Rayleigh waves was found at ~15.81 MHz from the experimental result. The multiple peaks centred at around 31.64 MHz were assigned to the Sezawa wave mode. The corresponding velocities were calculated to be ~4743 and ~9492 mm s^{-1}, for both Rayleigh and Sezawa wave modes, respectively.

3.2 Effects of SAWs on *E. coli* and *S. aureus*

The bacteria growth curves of both *E. coli* and *S. aureus* under the standard growth conditions (*i.e.*, placed in a 37 °C incubator) are illustrated in Fig. 3(a). For the growth curve of *E. coli*, the cells enter the first lag phase in the first two to three hours. When the cells are adapted to their new environment, they begin to divide exponentially and enter into the exponential growth phase which is denoted as the period of up to 24 hours. As for the growth curve of *S. aureus*, the cells enter the first stage in the first 5–6 hours, and begin to divide exponentially and enter into the exponential growth phase after 12 hours. Once the nutrients in the medium are depleted, the bacterial culture enters a stationary phase which is denoted between 12 and 22 hours. Cultures in the stationary phase collect catabolic products in the environment over time, which then result in a slight decrease in the number of viable cells known as the death phase, denoted from 22 hours.[7]

Fig. 3(b) compares the growth results for the control group and test group of *E. coli* in the PDMS chamber when it was subjected to various SAW RF powers (from 0.23 W up to 14.1 W). As the RF power is increased, the CFU mL^{-1} readings are increased until at a certain RF power where the CFU mL^{-1} readings become decreased at approximately 3.21 W. With the further increase of the SAW power to above 6.64 W, there are no colonies of bacteria detected. The dramatic decrease in CFU readings for SAWs at higher powers can be explained by the possibility of SAWs disrupting the cell walls of *E. coli* upon SAW agitation and streaming, causing the strong inactivation effects. The acousto-thermal effect causes temperature changes, which might be detrimental for the bacteria growth. It should also be addressed that sonochemical reactions can result in the production of highly reactive radicals and molecular products when SAWs induce nanoscale acoustic cavitation in liquids,[51] thus the bacterial cells are stressed and growth is prevented. Fig. S1(a) in the ESI† compares the OD values for the control and test groups of *E. coli* in the PDMS chamber when subjected to various RF powers. It was observed that as the RF powers were increased, the OD values were increased minimally with a few fluctuations before they started decreasing at higher RF powers. This implies that with increasing RF powers, the bacterial growth was induced with SAWs *via* the increment of OD values, before they started to decrease at higher RF powers, revealing the bacterial inactivation effect. As compared to the control group, the OD values were observed to have similar readings with minor fluctuations.

Fig. 3(c) compares the bacterial growth results for the control group and test group of *S. aureus* when subjected to various RF powers (0.23 W to 4.01 W). Bacterial quantifications were observed to be similar to those of *E. coli*, with an increased cell number until the threshold of 4.01 W, where a decreased cell number, or no cell number was observed at higher RF powers. Fig. S1(b) in the ESI† compares the OD values for the control and test groups of *S. aureus* in the PDMS chamber when subjected to various RF powers (0.36 to 4.01 W). It was observed that as the RF powers were increased, the OD values were also observed to increase. When compared to the control group, the OD values were observed to increase minimally. Similarly to *E. coli*, with increasing RF powers, *S. aureus* bacterial growth was induced with SAWs *via* the increment of OD values. Fig. S2(a) to (d) in the ESI† present the confocal microscopy images of both the control and test groups at two different RF powers (*i.e.*, 0.23 and 7.8 W).

As mentioned above, another effect induced upon applying SAW powers is the strong acousto-thermal effect, which can increase the temperature of the liquid. Along with the mechanical vibrations from SAWs, enhanced temperature will have a significant effect on the bacteria's life cycle. The temperature readings against time up to 30 minutes at various applied SAW powers from 0.24 W to 6.76 W are presented in Fig. 3(d). Clearly the temperature is increased with the duration of SAW power, and the maximum temperature has reached 76.1 °C at the power of 6.76 W. It is worth mentioning that as the temperature readings for both 0.61 and 1.01 W were too dense, these two RF powers are not presented in Fig. 3(d). Comparing the CFU mL^{-1} readings obtained from Fig. 3(c), it can be implied that when the RF powers applied induced preferable temperature (for example, near 37 °C), it would promote the bacterial growth, and this was annotated with the increase in the CFU mL^{-1} values. However, when much higher RF powers are applied, significant acousto-thermal effects occur (along with strong agitation and streaming effects), and the temperature increase would become a detrimental effect for bacterial growth, hence eliminating them instead at higher RF powers due to the high temperatures induced. Moreover, both *E. coli* and *S. aureus* are mesophilic strains, with 37 °C as the optimum temperature, but can grow at temperatures ranging between 10 °C and 40 °C and 15 °C and 45 °C for *E. coli* and *S. aureus*, respectively.[52,53] However, extended exposure above 42 °C is not recommended for *S. aureus*.[53] As for *E. coli*, although it was reported that it can grow at temperatures up to 49 °C and was also observed to be alive at 53 °C,[52] it was demonstrated that *E. coli* is sensitive to heat treatment from 60 °C to 70 °C which resulted in inactivation.[54] Hence, this further implies that the acousto-thermal effect from SAWs has an effect on the bacteria.

3.3 Enhancing the SAW effect with added ZnO tetrapods

Bacterial quantifications under different ZnO tetrapod concentrations at five RF powers are presented in Fig. 4(a) to (e). The CFU mL^{-1} readings for both the control

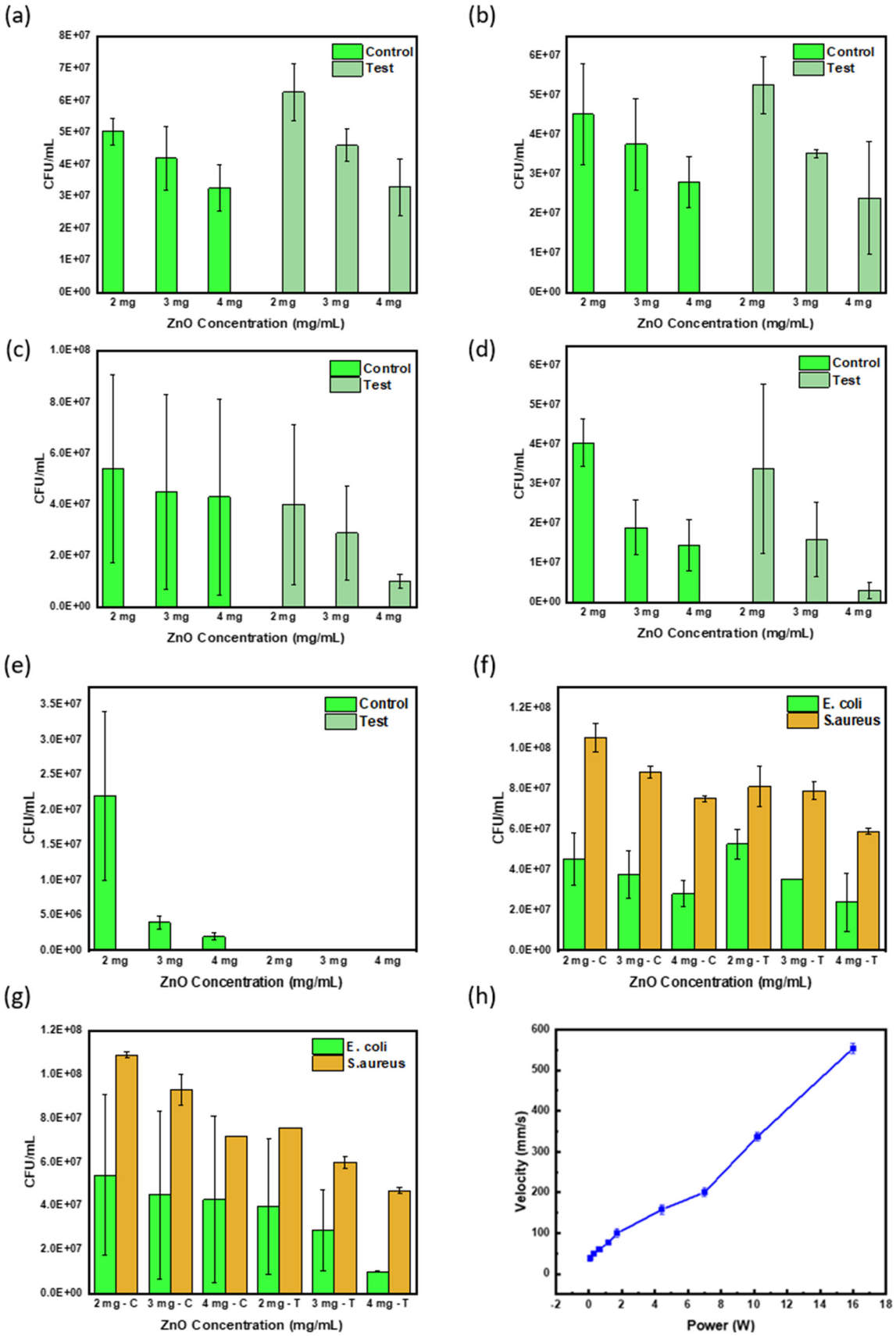

Fig. 4 CFU mL^{-1} readings at different ZnO concentrations with an RF power of (a) 0.36 W, (b) 0.95 W, (c) 1.4 W, (d) 1.9 W, and (e) 4.01 W. Comparison to *S. aureus* at (f) 1.4 W and (g) 1.9 W. (h) Acoustic streaming of bacteria solution in terms of velocity (mm s^{-1}) *versus* power (W) upon SAW agitation when subjected to various RF powers.

and test groups do not differ significantly at an RF power of 0.36 W and 0.95 W for *E. coli*. The main reason for this observation could be due to the insufficient SAW agitation to promote the interaction between the ZnO tetrapods and bacteria. In addition to this, the temperature increment induced by the SAWs in such a power range might also be insufficient to promote any growth or killing to occur.

As the ZnO concentration increases as depicted in Fig. 4(c) and (d), the CFU mL^{-1} readings were observed to decrease in the SAW test groups, which implies that SAW induced agitation and streaming effects enhanced the interactions of ZnO tetrapods with bacteria and promoted the inactivation mechanism. Upon the application of a higher RF power of 4.01 W as shown in Fig. 4(e), the SAW test group does not show any CFU values which indicates that SAWs dramatically enhanced the ZnO inactivation effect on bacteria growth, along with the acousto-thermal effect induced by SAWs. As a general trend, at lower ZnO concentrations, higher CFU mL^{-1} readings were observed before they started to decrease as the RF powers and ZnO concentrations were increased. When there was no presence of ZnO tetrapods, the CFU mL^{-1} values were observed to increase with increasing RF powers. However, the CFU mL^{-1} values began to decrease with increasing ZnO concentrations and RF powers. This further implies that there is a synergetic effect between the ZnO concentration and RF power on the antibacterial properties for *E. coli*, along with the accompanied acousto-thermal effect induced by SAWs. As compared to *S. aureus* as presented in Fig. 4(f) and (g), a similar trend was obtained to that of *E. coli* whereby as the RF powers were increased with increasing ZnO concentration, the CFU mL^{-1} readings were observed to decrease.

3.4 Discussions on mechanisms for bacteria inactivation

SAW effects on *E. coli* and *S. aureus*. The quantification results of *E. coli* show an increased number of CFU mL^{-1} with increasing RF powers. The increase in the CFU readings for the SAW test groups could be explained with the increase in liquid convection *via* three mechanisms. One of the mechanisms is known as the acoustic streaming (or internal flow) where the momentum from the propagating sound waves is being transferred to the liquid, resulting in the liquid to flow in the direction of the propagating sound waves and providing more nutrients and other supplies for bacteria growth.[22,23,55,56] Another mechanism is the SAW agitation or radiation effects on bacteria. SAWs can cause bacteria vibration, which can serve as an energy source to promote growth by allowing bacteria to multiply faster alongside with obtaining more nutrients from the streaming of the LB broths upon SAW agitation.[57]

The localised acousto-heating effect induced by the application of RF powers is another key factor for the life modulation of bacteria. At very low RF powers, the acousto-thermal effects are insignificant, thus there is no apparent bacteria growth enhancement. However, with the increase of SAW power, the acousto-thermal effects are increased significantly, which could encourage the bacterial growth. However, at very high RF powers, the induced acousto-thermal effects would be so significant that SAWs inhibit or cause the death of bacteria cells.

Fig. 4(h) shows the experimentally obtained velocity readings against various RF powers as the bacteria solution in the PDMS chamber was subjected to SAW agitation. With an increase in the RF power applied on the ZnO/Si SAW device, the velocity of the acoustic streaming of bacteria solution is increased. In this case, acoustic streaming can be analysed quantitatively *via* the following equations:[34,58]

$$\frac{\partial p}{\partial t} + \tilde{N}\cdot(p\boldsymbol{v}) = 0, \tag{2}$$
$$p\frac{\P \boldsymbol{v}}{\P t} + p(\boldsymbol{v}\cdot\tilde{N})\boldsymbol{v} = -\tilde{N}p + \mu\tilde{N}^2\boldsymbol{v} + \left(\mu_b + \frac{\mu}{3}\right)\tilde{N}\tilde{N}\cdot\boldsymbol{v},$$

where $\boldsymbol{v}$ is the flow velocity, t is the time, p is the pressure of the fluid, and μ_b and μ are the bulk and shear viscosities of the fluid, respectively. The left-hand side of eqn (2) represents the inertia force per unit volume of fluid where the first term represents the unsteady acceleration, and the second term represents the convection acceleration.[33] On the right-hand side of eqn (2), the net forces per unit volume include the pressure and viscosity gradients, where these equations can be used with the boundary conditions and linear relationship between pressure (p) and mass density (ρ) to predict the motion of the fluid:[34,58]

$$p = {c_0}^2 r \tag{3}$$

where c_0 refers to the speed of sound in the fluid. Moreover, there are two components of liquid flow, *i.e.*, fluid acoustic motion and streaming motion. At lower RF powers, slow streaming of the bacterial solution is induced when the velocity of the acoustic component is considerably larger than the streaming component.[34,55] This is known as linear streaming where the convection acceleration can be ignored.[34,55] In addition to this, the effect of inertia on the streaming motion is insignificant as compared to viscous effects, and thus slow streaming happens when the flow is laminar.[34,55] However, at higher RF powers, fast streaming of the bacterial solution was induced when the streaming velocity is of the same order or greater than the acoustic component. Such streaming causes the bacteria to experience flowing, allowing the continuously supplied nutrients from the LB broth, thus promoting bacteria growth.

SAWs were utilised to loosen cell bunches created during the microbial cultivation phase.[59] This allows the improvement in nutrient utilization by the bacterial cells, resulting in increased cell biomass and better target substance output.[22,59] Due to this reason, SAWs enhance membrane permeability, and this results in an increase in cell growth and multiplication by speeding up the transport of chemicals.[22,60] Moreover, SAWs can be utilized to modify the culture medium for the creation of an ideal environment for microbial growth and proliferation.

In other words, SAWs have effects on cellular components, functioning, and genetics, which further allow micro-organisms to multiply faster.[22,61]

Another possibility from SAWs would be the cavitation bubble-driven strategy where continuous motion of particles can be propelled by cavitation of bubbles during SAW agitation.[62,63] In this mechanism, the cavitation bubbles grow and collapse continuously which result in the generation of periodic pulse thrust to drive the particles or cells to move in the liquid.[62,63] In this manner, it would suggest that upon SAW agitation at various RF powers, SAWs can allow the ZnO tetrapods to interact with bacteria in LB broth to facilitate either growth or inactivation. It was also noted that cavitation bubbles can expand spherically and collapse asymmetrically, which makes it push on the particle generated by the bubble expansion which is greater than the pull on the particle generated by the bubble collapse.[62,63] However, as is well-known, the higher frequency would be difficult to cause effective generation of bubbles, and the higher the frequency, the smaller the bubbles. Therefore, such a cavitation effect should not be a key mechanism for the bacterial inactivation.[64]

Effects of ZnO tetrapods. Upon the addition of ZnO tetrapods without applying SAWs (*i.e.*, the control group), the CFU mL^{-1} readings were observed to decrease with increasing ZnO concentrations; these ZnO tetrapods interact with *E. coli* bacteria causing the reduction of bacteria.[65,66] With the introduction of SAW agitation at various RF powers, it induced acoustic streaming, enhancing the strong interaction/reactions between the ZnO tetrapods and *E. coli* bacteria. Other than acoustic streaming, it is presumed that the forces on particles exposed to acoustic waves are those induced by direct irradiation of the acoustic field and indirect irradiation from the scattering of the acoustic field from other particles.[34,67] The primary acoustic radiation pressure (F^{ARF}) is the force applied on a single particle in a fluid due to SAWs, whereas the secondary acoustic radiation pressure is about the force due to the acoustic interactions with other particles in the fluids.[34,67] The surface integral of the time-averaged second-order pressure p_2 and the momentum flux tensor $p_2\boldsymbol{v}_1\boldsymbol{v}_1$ at a fixed surface outside the oscillating sphere is used to calculate the acoustic radiation force.[68] Consequently, the general solution can be expressed as:

$$F^{ARF} = -\int_{\partial\Omega} da\{\langle p_2\rangle \boldsymbol{n} + p_0\langle(\boldsymbol{n}\cdot\boldsymbol{v}_1)\boldsymbol{v}_1\rangle\} \quad (4)$$

where $\boldsymbol{n}$ is the unit normal vector of the particle surface directed into the fluid. In general, the bacterial solution and ZnO tetrapods are exposed to the net acoustic radiation force and the SAW acoustic streaming induced Stokes drag force F^{drag} where the dominant force is dependent on the size of the particles.[34,57,69,70] Hence, particles that are larger than a given threshold size are typically dominated by the acoustic radiation force, and the size threshold is dependent on several factors such as the acoustic frequency, acoustic contrast factor, and kinematic viscosity.[34,57,69,70] The Stokes drag force, F^{drag}, is influenced by the fluid flow field, fluid viscosity, and particle size and shape. Consequently, F^{drag} is governed by the following equation for a spherical particle of radius r, with medium viscosity η and relative velocity $\boldsymbol{v}$:[68]

$$F^{drag} = 6\eta r\boldsymbol{v} \quad (5)$$

Considering that the PDMS chamber consists of bacterial solution and ZnO tetrapods, the acoustic waves are presumed to attenuate the boundary interaction with the PDMS walls, leading to boundary-driven streaming. When an acoustic wave propagates towards a solid boundary, the non-slip boundary will create a high-velocity gradient which is perpendicular to the solid surface, thus creating a steady boundary layer vorticity.[34,57,69,70] This is well-known as the inner boundary streaming.[34,57,69,70] The stronger the inner boundary streaming flow, the more counter-rotating streaming vortices are generated within the fluid.[34,57,69,70] This is referred to as outer boundary streaming or Rayleigh streaming.[34,57,69,70] In brief, SAW agitation allows the interaction of ZnO tetrapods with bacterial solution due to acoustic streaming and acoustic radiation force, as well as acousto-thermal effects.

Integrated effects of SAWs and ZnO micro- and nano-tetrapods. A decrease in CFU readings was observed when the bacteria solution was subjected to ZnO tetrapods. ZnO is known to be a transition metal oxide and a semiconductor with a wide band gap of 3.37 eV.[71–73] When the radiation energy is greater than the bandgap of ZnO, electron–hole pairs are created where the electrons will be promoted to the conduction band (CB).[74,75] The hole which is generated in the valence band (VB) will possess a strong oxidising character, and oxidising sites will be created which are capable of oxidising water molecules or hydroxide anions, thus generating strong oxidising species.[74,75] This reaction can then result in the redox chain reaction with the creation of reactive oxygen species (ROS) formed *via* hydroxyl radicals (OH^-), hydroperoxide radicals (HO_2^-) and superoxide radical anions (O_2^-) as pathways of bactericidal action, and this can be represented in the following equation:[73]

$$ZnO\ (s) + H^+\ ions\ (gas) \rightarrow Zn^+\ ions\ (solid) + H_2O\ (gas) \quad (6)$$

ZnO tetrapods can react with hydrogen ions (which can be from the DI water of the LB broth) to produce molecules of H_2O_2 and the generated H_2O_2 can penetrate the cell membrane and thus kill the bacteria. The generation of H_2O_2 is strongly dependent on the surface area of the ZnO tetrapods, which leads to more oxygen species. Hence, the generation of reactive oxygen species (ROS) could be one major factor that caused cell wall damage due to localised ZnO interactions, enhanced membrane permeability, internalization of nanoparticles due to the loss of proton motive force and uptake of toxic dissolved zinc ions.[73,74]

The other possibility could be that ZnO particles kill the bacterial cells *via* inducing oxidative stress where the increase in oxidative substances produced in the internal and external

environment of cells can cause damage to intracellular biomolecules.[74] In other words, oxidative stress can be induced by the ROS generation produced from ZnO tetrapods, which then results in the inhibition of protein synthesis and DNA replication. This electronic excitation can in turn destabilise the charges present in the cytoplasmic membrane of the bacterial cell, causing rupture. Therefore, ZnO can damage the cytoplasmic membrane by releasing Zn^{+} ions from the dissolution of ZnO in aqueous solution where the Zn^{+} ions are toxic to microbial cells and can damage important biological molecules such as cell membranes, proteins, and nucleic acids, leading to microbial death.[73,74]

4. Conclusions

Both active and passive methods were utilized to study the mechanisms and interactions of SAWs with bacteria solution and ZnO tetrapods. This was achieved through the concept of incorporating various concentrations of ZnO tetrapods with various RF powers. Our results revealed that increasing ZnO concentrations and RF powers resulted in the inactivation of bacteria, which was characterized by a low CFU mL^{-1} reading. The decrease in CFU mL^{-1} reading is mainly due to the synergistic effects of acoustic streaming, acoustic radiation force from SAWs and the generation of ROS species and oxidative stress induced by ZnO tetrapods upon SAW agitation at various RF powers.

Data availability

No primary research results, software, or code have been included and no new data were generated or analysed as part of this review. The datasets generated during and/or analysed during the current study are available from the corresponding author on reasonable request.

Author contributions

Huiling Ong: writing – original draft preparation, writing – review and editing, investigation, visualisation; Bruna Martins Dell' Agnese: writing – review and editing, investigation; Yunhong Jiang: review and editing, supervision, resources, validation; Yihao Guo: writing – review and editing, visualisation; Jian Zhou: writing – review and editing; Jikai Zhang: writing – review and editing; Jingting Luo: review and editing, validation; Ran Tao: review and editing, validation; Meng Zhang: writing – review and editing, validation; Lynn G. Dover: review and editing, supervision, resources, validation; Darren Smith: review and editing, validation; Kunyapat Thummavichai: writing – review and editing, validation, supervision; Yogendra Kumar Mishra: writing – review and editing, validation, resources; Qiang Wu: writing – review and editing, supervision; Yong-Qing Fu: conceptualization, methodology, validation, supervision, resources, writing – review and editing.

Conflicts of interest

There are no conflicts to declare.

Acknowledgements

This work was financially supported by the UK Engineering and Physical Sciences Research Council (EPSRC) under grant EP/P018998/1, Newton Mobility Grant (IE161019) through Royal Society, the National Natural Science Foundation of China (11504291, 52075162, 12104320), the Research Project in Fundamental and Application Fields of Guangdong Province (2020A1515110561), the Shenzhen Science & Technology Project (RCBS20200714114918249), the Innovation Leading Program of New and High-tech Industry of Hunan Province (2020GK2015), the Natural Science Foundation of Hunan Province (2021JJ20018), and the Natural Science Foundation of Changsha (kq2007026). YKM acknowledges the funding from the NANOCHEM (national infrastructure UFM 5229-00010B, NANOCHEM, Denmark).

References

1 J. D. Loike, *et al.*, Surface Acoustic Waves Enhance Neutrophil Killing of Bacteria, *PLoS One*, 2013, **8**(8), 2–8, DOI: **10.1371/journal.pone.0068334**.

2 Z. Kazan, *et al.*, Effective Prevention of Microbial Biofilm Formation on Medical Devices by Low-Energy Surface Acoustic Waves, *Antimicrob. Agents Chemother.*, 2006, **50**(12), 4144, DOI: **10.1128/AAC.00418-06**.

3 M. Kopel, E. Degtyar and E. Banin, Surface acoustic waves increase the susceptibility of Pseudomonas aeruginosa biofilms to antibiotic treatment, *Biofouling*, 2011, **27**(7), 701–711, DOI: **10.1080/08927014.2011.597051**.

4 S. Markowitz, J. Rosenblum, M. Goldstein, H. P. Gadagkar and L. Litman, The Effect of Surface Acoustic Waves on Bacterial Load and Preventing Catheter-associated Urinary Tract Infections (CAUTI) in Long Term Indwelling Catheters, *Medical & Surgical Urology*, 2018, **7**(4), 1–5, DOI: **10.4172/2168-9857.1000210**.

5 Y. Qiu, Y. Zhou, Y. Chang, X. Liang, H. Zhang, X. Lin, K. Qing, X. Zhou and Z. Luo, The Effects of Ventilation, Humidity, and Temperature on Bacterial Growth and Bacterial Genera Distribution, *Int. J. Environ. Res. Public Health*, 2022, **19**(22), 15345, DOI: **10.3390/IJERPH192215345**.

6 S. Finn, O. Condell, P. McClure, A. Amézquita and S. Fanning, Mechanisms of survival, responses and sources of Salmonella in low-moisture environments, *Front. Microbiol*, 2013, **4**, 331, DOI: **10.3389/FMICB.2013.00331**.

7 P. Pletnev, I. Osterman, P. Sergiev, A. Bogdanov and O. Dontsova, Survival guide: Escherichia coli in the stationary phase, *Acta Naturae*, 2015, **7**(4), 22, DOI: **10.32607/20758251-2015-7-4-22-33**.

8 J. W. Tang, The effect of environmental parameters on the survival of airborne infectious agents, *J. R. Soc., Interface*, 2009, **6**(SUPPL. 6), 737–746, DOI: **10.1098/RSIF.2009.0227.FOCUS**.

9 S. Qin, K. Xu, B. Nie, F. Ji and H. Zhang, Approaches based on passive and active antibacterial coating on titanium to achieve antibacterial activity, *J. Biomed. Mater. Res., Part A*, 2018, **106**(9), 2531–2539, DOI: **10.1002/JBM.A.36413**.

10 A. Uneputty, *et al.*, Strategies applied to modify structured and smooth surfaces: A step closer to reduce bacterial adhesion and biofilm formation, *Colloid Interface Sci. Commun.*, 2022, **46**, 100560, DOI: **10.1016/J.COLCOM.2021.100560**.

11 W. Ahmed, Z. Zhai and C. Gao, Adaptive antibacterial biomaterial surfaces and their applications, *Mater. Today Bio*, 2019, **2**, 100017, DOI: **10.1016/J.MTBIO.2019.100017**.

12 X. M. Yang, J. W. Hou, Y. Tian, J. Y. Zhao, Q. Q. Sun and S. B. Zhou, Antibacterial surfaces: Strategies and applications, *Sci. China: Technol. Sci.*, 2022, **65**(5), 1000–1010, DOI: **10.1007/s11431-021-1962-x**.

13 Z. Li and K. Aik Khor, Preparation and Properties of Coatings and Thin Films on Metal Implants, *Encycl. Biomed. Eng.*, 2019, vol. 1–3, pp. 203–212, DOI: **10.1016/B978-0-12-801238-3.11025-6**.

14 M. K. Chug and E. J. Brisbois, Recent Developments in Multifunctional Antimicrobial Surfaces and Applications toward Advanced Nitric Oxide-Based Biomaterials, *ACS Mater. Au*, 2022, **2**(5), 525–551, DOI: **10.1021/ACSMATERIALSAU.2C00040/ASSET/IMAGES/LARGE/MG2C00040_0014.JPEG**.

15 M. Skwarczynski, S. Bashiri, Y. Yuan, Z. M. Ziora, O. Nabil, K. Masuda, M. Khongkow, N. Rimsueb, H. Cabral, U. Ruktanonchai, M. A. T. Blaskovich and I. Toth, Antimicrobial Activity Enhancers: Towards Smart Delivery of Antimicrobial Agents, *Antibiotics*, 2022, **11**(3), 412, DOI: **10.3390/antibiotics11030412**.

16 J. Lei, L. Sun, S. Huang, C. Zhu, P. Li, J. He, V. Mackey, D. H. Coy and Q. He, The antimicrobial peptides and their potential clinical applications, *Am. J. Transl. Res.*, 2019, **11**(7), 3919–3931.

17 R. H. Vafaie and H. Heidarzadeh, AC electrothermal assisted plasmonic biosensor for detection of low-concentration biological analytes, *Opt. Laser Technol.*, 2021, **140**, 107078, DOI: **10.1016/J.OPTLASTEC.2021.107078**.

18 S. Govindaraju, M. Ramasamy, R. Baskaran, S. J. Ahn and K. Yun, Ultraviolet light and laser irradiation enhances the antibacterial activity of glucosamine-functionalized gold nanoparticles, *Int. J. Nanomed.*, 2015, **10**(Spec Iss), 67, DOI: **10.2147/IJN.S88318**.

19 C. H. Chen and T. K. Lu, Development and Challenges of Antimicrobial Peptides for Therapeutic Applications, *Antibiotics*, 2020, **9**(1), 24, DOI: **10.3390/ANTIBIOTICS9010024**.

20 P. Tan, H. Fu and X. Ma, Design, optimization, and nanotechnology of antimicrobial peptides: From exploration to applications, *Nano Today*, 2021, **39**, 101229, DOI: **10.1016/J.NANTOD.2021.101229**.

21 R. Abbasi, G. Shineh, M. Mobaraki, S. Doughty and L. Tayebi, Structural parameters of nanoparticles affecting their toxicity for biomedical applications: a review, *J. Nanopart. Res.*, 2023, **25**(3), 1–35, DOI: **10.1007/S11051-023-05690-W**.

22 G. Huang, *et al.*, Effects of ultrasound on microbial growth and enzyme activity, *Ultrason. Sonochem.*, 2017, **37**, 144–149, DOI: **10.1016/J.ULTSONCH.2016.12.018**.

23 W. G. Pitt and S. A. Ross, Ultrasound increases the rate of bacterial cell growth, *Biotechnol. Prog.*, 2003, **19**(3), 1038–1044, DOI: **10.1021/bp0340685**.

24 S. Gu, Y. Zhang and Y. Wu, Effects of sound exposure on the growth and intracellular macromolecular synthesis of E. coli k-12, *PeerJ*, 2016, (4), 1920, DOI: **10.7717/peerj.1920**.

25 A. Behzadnia, M. Moosavi-Nasab, S. Ojha and B. K. Tiwari, Exploitation of Ultrasound Technique for Enhancement of Microbial Metabolites Production, *Molecules*, 2020, **25**(22), 5473, DOI: **10.3390/MOLECULES25225473**.

26 L. Huan, J. Yiying, R. B. Mahar, W. Zhiyu and N. Yongfeng, Effects of ultrasonic disintegration on sludge microbial activity and dewaterability, *J. Hazard. Mater.*, 2009, **161**(2–3), 1421–1426, DOI: **10.1016/J.JHAZMAT.2008.04.113**.

27 L. M. Carrillo-Lopez, *et al.*, Recent advances in the application of ultrasound in dairy products: Effect on functional, physical, chemical, microbiological and sensory properties, *Ultrason. Sonochem.*, 2021, **73**, 105467, DOI: **10.1016/J.ULTSONCH.2021.105467**.

28 A. Chávez-Martínez, R. A. Reyes-Villagrana, A. L. Rentería-Monterrubio, R. Sánchez-Vega, J. M. Tirado-Gallegos and N. A. Bolivar-Jacobo, Low and High-Intensity Ultrasound in Dairy Products: Applications and Effects on Physicochemical and Microbiological Quality, *Foods*, 2020, **9**(11), 1688, DOI: **10.3390/FOODS9111688**.

29 Y. Huang, P. K. Das and V. R. Bhethanabotla, Surface acoustic waves in biosensing applications, *Sens. Actuators Rep.*, 2021, **3**, 100041, DOI: **10.1016/J.SNR.2021.100041**.

30 R. Tao, *et al.*, Flexible and Integrated Sensing Platform of Acoustic Waves and Metamaterials based on Polyimide-Coated Woven Carbon Fibers, *ACS Sens.*, 2020, **5**(8), 2563–2569, DOI: **10.1021/ACSSENSORS.0C00948/ASSET/IMAGES/LARGE/SE0C00948_0006.JPEG**.

31 H. Fallahi, J. Zhang, H. P. Phan and N. T. Nguyen, Flexible Microfluidics: Fundamentals, Recent Developments, and Applications, *Micromachines*, 2019, **10**(12), 830, DOI: **10.3390/MI10120830**.

32 Y. Q. Fu, *et al.*, Advances in piezoelectric thin films for acoustic biosensors, acoustofluidics and lab-on-chip applications, *Prog. Mater. Sci.*, 2017, **89**, 31–91, DOI: **10.1016/J.PMATSCI.2017.04.006**.

33 S. Damiati, U. B. Kompella, S. A. Damiati and R. Kodzius, Microfluidic Devices for Drug Delivery Systems and Drug Screening, *Genes*, 2018, **9**(2), 103, DOI: **10.3390/GENES9020103**.

34 M. Stringer, *et al.*, Methodologies, technologies, and strategies for acoustic streaming-based acoustofluidics, *Appl. Phys. Rev.*, 2023, **10**(1), 011315, DOI: **10.1063/5.0134646**.

35 H. Ong, *et al.*, ZnO/glass thin film surface acoustic waves for efficient digital acoustofluidics and active surface cleaning, *Mater. Chem. Phys.*, 2022, **287**, 126290, DOI: **10.1016/J.MATCHEMPHYS.2022.126290**.

36 D. Peng, W. Tong, D. J. Collins, M. R. Ibbotson, S. Prawer and M. Stamp, Mechanisms and Applications of Neuromodulation Using Surface Acoustic Waves—A Mini-Review, *Front. Neurosci.*, 2021, **15**, 27, DOI: **10.3389/FNINS.2021.629056**.

37 F. A. Duck, H. C. Starritt, G. R. Ter Haar and M. J. Lunt, Surface heating of diagnostic ultrasound transducers, *Br. J. Radiol.*, 2014, **62**(743), 1005–1013, DOI: **10.1259/0007-1285-62-743-1005**.

38 A. L. T. Killingback, V. R. Newey, M. A. El-Brawany and D. K. Nassiri, Development of a Thermal Test Object for the Measurement of Ultrasound Intracavity Transducer Self-Heating, *Ultrasound Med. Biol.*, 2008, **34**(12), 2035–2042, DOI: **10.1016/j.ultrasmedbio.2008.06.002**.

39 W. Zhong, W. H. Sit, J. M. F. Wan and A. C. H. Yu, Sonoporation induces apoptosis and cell cycle arrest in human promyelocytic leukemia cells, *Ultrasound Med. Biol.*, 2011, **37**(12), 2149–2159, DOI: **10.1016/j.ultrasmedbio.2011.09.012**.

40 M. Wiklund, Acoustofluidics 12: Biocompatibility and cell viability in microfluidic acoustic resonators, *Lab Chip*, 2012, **12**(11), 2018–2028, DOI: **10.1039/C2LC40201G**.

41 X. Yang and J. Jo, Enhanced cavitation by using two consecutive ultrasound waves at different frequencies, *Appl. Phys. Lett.*, 2014, **105**(19), 193701, DOI: **10.1063/1.4902118/596604**.

42 Z. Lin, *et al.*, On-Chip Ultrasound Modulation of Pyramidal Neuronal Activity in Hippocampal Slices, *Adv. Biosyst.*, 2018, **2**(8), 1800041, DOI: **10.1002/ADBI.201800041**.

43 J. Zhou, D. B. Xiao, Z. X. Song, M. Zhuo and X. Z. Wu, Transparent graphene-AZO/ZNO/glass surface acoustic wave device for electronics and lab-on-a-chip applications, *IEEE/LEOS Int. Conf. Opt. MEMS*, 2018, vol. 2018, pp. 79–82, DOI: **10.1109/MEMSYS.2018.8346487**.

44 H. L. Ong, *et al.*, Integrated transparent surface acoustic wave technology for active de-fogging and icing protection on glass, *Mater. Chem. Phys.*, 2023, **304**, 127842, DOI: **10.1016/J.MATCHEMPHYS.2023.127842**.

45 Z. Kazan, *et al.*, Effective prevention of microbial biofilm formation on medical devices by low-energy surface acoustic waves, *Antimicrob. Agents Chemother.*, 2006, **50**(12), 4144–4152, DOI: **10.1128/AAC.00418-06/ASSET/9E1E0270-D5D2-4EEC-BC78-2DE1676F3900/ASSETS/GRAPHIC/ZAC0120662000004.JPEG**.

46 N. S. L. Chew, C. W. Ooi, L. Y. Yeo and M. K. Tan, Influence of MHz-order acoustic waves on bacterial suspensions, *Ultrasonics*, 2024, **138**, 107234, DOI: **10.1016/J.ULTRAS.2023.107234**.

47 S. H. Hong, J. B. Gorce, H. Punzmann, N. Francois, M. Shats and H. Xia, Surface waves control bacterial attachment and formation of biofilms in thin layers, *Sci. Adv.*, 2020, **6**(22), 1–8, DOI: **10.1126/sciadv.aaz9386**.

48 X. Tao, *et al.*, Three-Dimensional Tetrapodal ZnO Microstructured Network Based Flexible Surface Acoustic Wave Device for Ultraviolet and Respiration Monitoring Applications, *ACS Appl. Nano Mater.*, 2020, **3**(2), 1468–1478, DOI: **10.1021/ACSANM.9B02300**.

49 Y. K. Mishra, *et al.*, Fabrication of Macroscopically Flexible and Highly Porous 3D Semiconductor Networks from Interpenetrating Nanostructures by a Simple Flame Transport Approach, *Part. Part. Syst. Charact.*, 2013, **30**(9), 775–783, DOI: **10.1002/PPSC.201300197**.

50 H. Papavlassopoulos, *et al.*, Toxicity of Functional Nano-Micro Zinc Oxide Tetrapods: Impact of Cell Culture Conditions, Cellular Age and Material Properties, *PLoS One*, 2014, **9**(1), e84983, DOI: **10.1371/JOURNAL.PONE.0084983**.

51 S. Kamineni and C. Huang, The antibacterial effect of sonication and its potential medical application, *SICOT-J*, 2019, **5**, 19, DOI: **10.1051/SICOTJ/2019017**.

52 U. Fotadar, P. Zaveloff and L. Terracio, Growth of Escherichia coli at elevated temperatures, *J. Basic Microbiol.*, 2005, **45**(5), 403–404, DOI: **10.1002/JOBM.200410542**.

53 D. M. Missiakas and O. Schneewind, Growth and Laboratory Maintenance of Staphylococcus aureus, *Curr. Protoc. Microbiol.*, 2013, **28**(1), 9C.1, DOI: **10.1002/9780471729259.MC09C01S28**.

54 G. Charimba, C. J. Hugo and A. Hugo, The growth, survival and thermal inactivation of Escherichia coli O157:H7 in a traditional South African sausage, *Meat Sci.*, 2010, **85**(1), 89–95, DOI: **10.1016/J.MEATSCI.2009.12.010**.

55 O. Bulliard-Sauret, S. Ferrouillat, L. Vignal, A. Memponteil and N. Gondrexon, Heat transfer enhancement using 2 MHz ultrasound, *Ultrason. Sonochem.*, 2017, **39**, 262–271, DOI: **10.1016/J.ULTSONCH.2017.04.021**.

56 B.-G. Loh, S. Hyun, P. I. Ro and C. Kleinstreuer, Acoustic streaming induced by ultrasonic flexural vibrations and associated enhancement of convective heat transfer, *J. Acoust. Soc. Am.*, 2002, **111**(2), 875–883, DOI: **10.1121/1.1433811**.

57 D. J. Collins, Z. Ma and Y. Ai, Highly Localized Acoustic Streaming and Size-Selective Submicrometer Particle Concentration Using High Frequency Microscale Focused Acoustic Fields, *Anal. Chem.*, 2016, **88**(10), 5513–5522, DOI: **10.1021/ACS.ANALCHEM.6B01069/SUPPL_FILE/AC6B01069_SI_004.AVI**.

58 Y. Q. Fu, *et al.*, Recent developments on ZnO films for acoustic wave based bio-sensing and microfluidic applications: a review, *Sens. Actuators, B*, 2010, **143**, 606–619, DOI: **10.1016/j.snb.2009.10.010**.

59 H. Wang, *et al.*, Application of ultrasonication at different microbial growth stages during apple juice fermentation by Lactobacillus plantarum: Investigation on the metabolic response, *Ultrason. Sonochem.*, 2021, **73**, 105486, DOI: **10.1016/J.ULTSONCH.2021.105486**.

60 L. Yuan, T. Wang, F. Xing, X. Wang and H. Yun, Enhancement of Anammox performances in an ABR at normal temperature by the low-intensity ultrasonic irradiation, *Ultrason. Sonochem.*, 2021, **73**, 105468, DOI: **10.1016/J.ULTSONCH.2021.105468**.

61 E. R. Ritenour, Ultrasound: Its Chemical, Physical, and Biological Effects, *Radiology*, 1989, **173**(1), 136, DOI: **10.1148/radiology.173.1.136**.

62 F. Xu, Y. Liu, M. Chen, J. Luo and L. Bai, Continuous motion of particles attached to cavitation bubbles, *Ultrason. Sonochem.*, 2024, **107**, 106888, DOI: **10.1016/J.ULTSONCH.2024.106888**.

63 M. Roudini, J. Manuel Rosselló, O. Manor, C. D. Ohl and A. Winkler, Acoustic resonance effects and cavitation in SAW aerosol generation, *Ultrason. Sonochem.*, 2023, **98**, 106530, DOI: **10.1016/J.ULTSONCH.2023.106530**.

64 L. Yeo, S. Leslie, Y. Yeo, S. Ramesan, A. R. Rezk and L. Y. Yeo, High frequency acoustic permeabilisation of drugs through tissue for localised mucosal delivery, *Lab Chip*, 2018, **18**(21), 3272–3284, DOI: **10.1039/C8LC00355F**.

65 H. Papavlassopoulos, *et al.*, Toxicity of Functional Nano-Micro Zinc Oxide Tetrapods: Impact of Cell Culture Conditions, Cellular Age and Material Properties, *PLoS One*, 2014, **9**(1), e84983, DOI: **10.1371/JOURNAL.PONE.0084983**.

66 A. Nasajpour, *et al.*, Nanostructured Fibrous Membranes with Rose Spike-Like Architecture, *Nano Lett.*, 2017, **17**(10), 6235–6240, DOI: **10.1021/ACS.NANOLETT.7B02929/ASSET/IMAGES/LARGE/NL-2017-02929P_0004.JPEG**.

67 J. Wu and W. L. Nyborg, Ultrasound, cavitation bubbles and their interaction with cells, *Adv. Drug Delivery Rev.*, 2008, **60**(10), 1103–1116, DOI: **10.1016/J.ADDR.2008.03.009**.

68 J. Friend and L. Y. Yeo, Microscale acoustofluidics: Microfluidics driven via acoustics and ultrasonics, *Rev. Mod. Phys.*, 2011, **83**(2), 647–704, DOI: **10.1103/REVMODPHYS.83.647**.

69 S. Li, F. Ma, H. Bachman, C. E. Cameron, X. Zeng and T. J. Huang, Acoustofluidic bacteria separation, *J. Micromech. Microeng.*, 2016, **27**(1), 015031, DOI: **10.1088/1361-6439/27/1/015031**.

70 P. B. Muller, R. Barnkob, M. J. H. Jensen and H. Bruus, A numerical study of microparticle acoustophoresis driven by acoustic radiation forces and streaming-induced drag forces, *Lab Chip*, 2012, **12**(22), 4617–4627, DOI: **10.1039/C2LC40612H**.

71 H. L. Ong, *et al.*, Doped tungsten oxide microstructures for enhancing ultraviolet sensing based on ZnO/glass transparent acoustic wave technology, *Sens. Actuators, A*, 2023, **363**, 114705, DOI: **10.1016/J.SNA.2023.114705**.

72 E. Manikandan, *et al.*, Zinc oxide epitaxial thin film deposited over carbon on various substrate by pulsed laser deposition technique, *J. Nanosci. Nanotechnol.*, 2010, **10**(9), 5602–5611, DOI: **10.1166/JNN.2010.2478**.

73 C. R. Mendes, *et al.*, Antibacterial action and target mechanisms of zinc oxide nanoparticles against bacterial pathogens, *Sci. Rep.*, 2022, **12**(1), 1–10, DOI: **10.1038/s41598-022-06657-y**.

74 A. Sirelkhatim, *et al.*, Review on Zinc Oxide Nanoparticles: Antibacterial Activity and Toxicity Mechanism, *Nano-Micro Lett.*, 2015, **7**(3), 219, DOI: **10.1007/S40820-015-0040-X**.

75 F. J. Serrao, N. N. Bappalige, K. M. Sandeep and S. Raghavendra, Dominance of c-axis orientation on the carrier transport properties of Sn doped ZnO thin films, *Thin Solid Films*, 2021, **722**, 138579, DOI: **10.1016/J.TSF.2021.138579**.

